# Removal of hazardous textile dyes from water using Ni impregnated ZnO through sonophotocatalytic degradation

Fatima Khitab, Muhammad Rasul Jan, Jasmin Shah*

*Institute of Chemical Sciences, University of Peshawar, Peshawar 25120, Khyber Pakhtunkhwa, Pakistan, Tel./Fax: 092-91-9216652;
emails: jasminshah2001@yahoo.com (J. Shah), fatima_khitab@yahoo.com (F. Khitab), rasuljan@yahoo.com (M. Rasul Jan)*

## ABSTRACT

The visible-light-induced semiconductor photocatalyst nickel (Ni) impregnated ZnO was prepared by the wet impregnation method. Impregnation of Ni on ZnO shifts the bandgap from UV to the visible region. The present study involves the sonophotocatalytic degradation of textile dyes Acid Violet 49 (AV-49) and Acid Blue 45 (AB-45) in the presence of Ni–ZnO photocatalyst under the irradiation of visible light. The degradation efficiency of sonophotocatalysis was higher than sonolysis, sonocatalysis, photolysis and photocatalysis. The photocatalyst was characterized by scanning electron microscopy, energy-dispersive X-ray analysis and X-ray diffraction. Effect of different operational parameters such as pH, catalyst dosage, oxidizing agents (enhancers), initial dye concentration, scavengers, catalyst re-usability, catalyst settling time and catalyst poisoning were studied. Maximum degradation (100%) of AV-49 and AB-45 was found at pH 10 in 20 min. The re-usability of the photocatalyst test showed an increase in time of degradation from 20 to 60 min with a 10%–20% decrease in degradation efficiency. The degradation of AV-49 and AB-45 follows the pseudo-first-order kinetic model. The results of sonophotocatalytic degradation of textile dyes were attributed to the efficient absorption of visible light, separation of charge carriers and good surface area. The method of sonophotocatalytic degradation assisted with the oxidizing agents has also advantages like safety, high efficiency and economy if applied to the textile dye wastewater treatment.

*Keywords:* Sonophotocatalysis; Impregnated ZnO; Photocatalyst; Textile dyes; Degradation

## 1. Introduction

Semiconductor photocatalysts have been used from the last few years for the removal via the degradation process of various pollutants from water and wastewater samples. Among the photocatalysts, $TiO_2$ and ZnO are the most common semiconductor photocatalyst applied for different photocatalytic processes. The photocatalytic activity and photophysical functions of these photocatalysts have been increased further by doping with non-metals [1], metals [2], rare earth metals [3], transition metals [4–6] and by coupling with a metal oxide such as ZnO/CuO, CdO/ZnO, $NiFe_2O_4$/ZnO [7–9]. In photocatalytic, degradation of organic pollutants modified semiconductors played an important role. A combination of various semiconductors may decrease the required energy of the bandgap and can shift absorbance of the new photocatalyst to longer wavelength region and achieve the greater photocatalytic activity.

ZnO photocatalyst in a pure form has certain limitations such as the fast rate of recombination of the pairs of electron-hole ($e^- – h^+$) generated. Thus, to increase the activity of ZnO, the recombination of electron-hole pairs have to be blocked. Therefore, surface modification or doping of semiconductors with metal ions has been considered as a possible way in the reduction of the recombination of the electron-hole pair [3]. It is accepted largely that ZnO

* Corresponding author.

when doped or impregnated with transition metal cations it changes the Zn coordination environment in the lattice and changes the structure of the electronic energy band of ZnO. The trapping sites are now metal ions that accept the electrons or holes which are photogenerated from the ZnO. Recombinations of the carriers are prevented and thus improve the material photocatalytic activity. Hence, ZnO was modified with transition metal cations to increase its photocatalytic activity by trapping sites to enhance the activity of photocatalyst and slow down the rate of recombination of electron-hole pair [5,10].

From the last few years, different processes like sonocatalysis and photocatalysis have been used for the treatment of dye wastewater samples [11,12] along with an increase in the process of sonophotocatalytic for degradation and removal of textile dyes. In the photocatalytic process, pairs of electron-hole are produced in a semiconductor photocatalyst by photon and then generate free radicals. Otherwise, in the sonocatalytic process, cavitation bubbles are produced by ultrasonic waves which collapse rapidly. The high energy liberated from cavitation bubbles leads to the formation of electron-hole pairs in a semiconductor photocatalyst and which in turn generates free radicals. When the two systems combine in the form of sonophotocatalysis, the synergistic effect of ultrasonic waves provides extra cavitation energy and speeds up the photocatalytic degradation process [4,5].

In the present work, the photocatalyst (ZnO) was modified by impregnation with nickel (Ni–ZnO) to enhance the photocatalytic efficiency of ZnO in the visible spectrum of electromagnetic radiation and decrease the time of degradation in the presence of ultrasonic waves. On the basis of the literature study, no data was found on the application of Ni–ZnO photocatalyst for the sonophotocatalytic degradation of Acid Violet 49 (AV-49) and Acid Blue 45 (AB-45) dyes. Conditions for sonophotocatalytic degradation of AV-49 and AB-45 dyes were investigated and the degradation mechanism was explained.

## 2. Materials and methods

### 2.1. Material

Zinc oxide (ZnO), nickel nitrate ($Ni(NO_3)_2$), hydrogen peroxide ($H_2O_2$), sodium perchlorate ($NaClO_4$) and potassium peroxydisulphate ($K_2S_2O_8$) were supplied by BDH Laboratory Supplies, Poole, BH15 1TD, England. Acid Violet 49 (molecular formula = $C_{39}H_{40}N_3NaO_6S_2$, colour index number = 42535, $\lambda_{max}$ = 550 nm) and Acid Blue 45 (molecular formula = $C_{14}H_8N_2Na_2O_{10}S_2$, colour index number = 63010, $\lambda_{max}$ = 590 nm) dyes (Table S3) were obtained from Merck (Darmstadt, Germany). Britton–Robinson buffer [13] was used to adjusted the pH of the dye solutions. All chemicals used were of analytical grade purity.

### 2.2. Photocatalyst preparation

The metal impregnated zinc oxide (ZnO) photocatalyst was synthesized by a wet impregnation process following the method described in our previous work [14]. The concentration of salt ($Ni(NO_3)_2$) was calculated on the basis of the weight of metal at a known weight of ZnO. The nickel-metal salt was dissolved in a suitable amount of water and poured into the slurry of ZnO. After stirring at 900 rpm for 1 h at 60°C then the slurry was filtered, washed and dried for 6 h at 110°C in an oven. Finally, calcined at 300°C in a furnace for 6 h and cooled in a desiccator. The dried sample was ground to powder and pass through the mesh to a particle size ≤150 μm.

### 2.3. Instrumentation

For absorbance measurement, UV/Vis spectrophotometer with 1 cm glass matched cells (Model SP-3000 plus, Optima, Japan), was used at maximum wavelength of 585 and 615 for AV-49 and AB-45, respectively. Kumsung ultrasonic bath with 40 kHz frequency was used for ultrasonic waves. Tungsten filament lamp of 200 W was used as a source of visible radiation for photocatalytic degradation of dyes.

The surface morphology of ZnO and impregnated Ni–ZnO was determined using scanning electron microscopy (SEM, model JSM5910) of JEOL, Japan. Elemental compositions of ZnO and Ni–ZnO photocatalysts were determined with energy-dispersive X-ray (EDX) spectroscopy. $N_2$ adsorption/desorption method was used for surface area analysis by surface area analyzer (Quantachrome, Nova Station, A). X-ray diffractometer (model JDX-9C) of JEOL (Japan) was used at room temperature for phase analysis with monochromatic Cu-K$\alpha$ radiation ($\lambda$ = 1. 5418 Å) and 30 mA in the 2θ from 10° to 80° with 1.03°/min at 40 KV. The spectrophotometric method with the help of the Tauc plot was used for the determination of the bandgap energy of ZnO and Ni–ZnO. Transmission (%) spectrum of 0.05% sample suspension was measured in the range of 200–900 nm. Absorbance was calculated using $A = 2 - \log \%T$, and absorbance of the sample was multiplied by photon energy hυ (ev), then the plot was drawn between $(Ah\upsilon)^2$ (direct bandgap) as a function of hυ (ev).

### 2.4. Experiment for photocatalytic degradation

In the photocatalytic degradation experiment, the activity of the prepared photocatalyst was evaluated by studying the degradation of textile dyes in aqueous solution at room temperature under irradiation of visible light using tungsten lamp. Dye solutions of AV-49 and AB-45 (100 mL) with the desired initial concentration (10 mg L$^{-1}$) were mixed with 0.2 g L$^{-1}$ of photocatalyst (ZnO and Ni–ZnO) in a photoreactor. To ensure the dye adsorption–desorption balance on the surface of ZnO and Ni–ZnO, the suspension was placed in the dark for 30 min in a photoreactor. After this, the pH of the suspension was adjusted to 10 and then 5 mmol solutions of $H_2O_2$ was added. To avoid scattering of light, the photoreactor was placed inside a wooden box and the interior of the box was laminated with aluminum foil to enhance light reflection. By illumination with a tungsten filament lamp, the photocatalytic degradation process was initiated. After a specified time period, an aliquot of the dye solution (5 mL) was sampled and centrifuged for 30–45 min at 1,500 rpm to remove dispersed photocatalyst. After centrifugation, the clear resultant dye solution was analyzed for dye concentration present (AV-49 and AB-45) using a UV-Vis spectrophotometer with the respective optimum

wavelength ($\lambda_{max}$) of each dye. Using Eq. (1) the efficiency of degradation was calculated.

$$\% \text{ Degradation} = \frac{C_0 - C_f}{C_0} \times 100 \qquad (1)$$

where $C_0$ and $C_f$ are the initial and final concentrations of the dye (AV-49 and AB-45) solution after time $t$ irradiation. All degradation experiments of dyes were performed in triplicate. The conditions for degradation of dyes were investigated by varying pH, photocatalyst amount, oxidizing agent, radical scavenger and initial dye (AV-49 and AB-45) concentration under photocatalytic degradation. The schematic presentation is shown in Fig. 1.

## 2.5. Sonophotocatalytic study

The optimized conditions of photocatalytic degradation of dyes were used in the sonophotocatalytic degradation method. Briefly, AV-49 and AB-45 dye solution (100 mL) of 10 mg $L^{-1}$ concentration was mixed with 0.2 g $L^{-1}$ of photocatalyst (ZnO and Ni–ZnO) in a photoreactor. The suspension pH was adjusted to 10 and then 5 mmol of $H_2O_2$ solution was added. The dye solution under the tungsten filament lamp was placed in an ultrasonic bath (40 kHz ultrasonic waves) for sonophotocatalytic degradation. The sonophotocatalytic experiments were carried out in triplicate. For determination and calculation of the percent degradation of dye, the same calculations were used as in the case of the photocatalytic degradation process.

The photocatalytic degradation was also performed using Ni–ZnO photocatalyst at optimum conditions in the same reactor with irradiation of sunlight from 11:00 am to 3:00 pm (~400 W m$^{-2}$).

## 3. Results and discussions

### 3.1. Photocatalyst characterization

To know the morphology of the photocatalyst it was analyzed by SEM as well as to confirm the dispersion of nickel onto the ZnO surface after impregnation. Fig. 2 depicted the topography of pure ZnO, nickel impregnated ZnO, five times re-used impregnated ZnO (Ni–ZnO) and re-used impregnated photocatalyst after washing. As can be seen that the topography of ZnO support changed after impregnation with nickel and different shapes of small particles are present onto the ZnO particles surface. The topography of five time's re-used photocatalyst also shows that Ni particles impregnated on ZnO.

Fig. 3 shows the EDX spectra for pure ZnO, modified with nickel, re-used after five times modified and re-used Ni–ZnO photocatalyst after washing. The spectra of Fig. 3b shows the presence of nickel which indicated the modification of ZnO with nickel. Fig. 2c shows the nickel concentration after five times repeatedly use of Ni–ZnO photocatalyst for degradation process which shows that the nickel concentration changes in the modified ZnO are negligible.

The X-ray diffraction (XRD) for ZnO, Ni–ZnO and five times re-used Ni–ZnO and after washing is given in (Fig. S1). In Fig. S1, the spectra (S1a) is of ZnO with its pattern according to ICDD number 11136, 30888, 361451 and 11244 shows a peak at 28°, 31°, 32°, 34°, 36°, 47°, 50°, 56°, 62°, 66°, 67° and 69°, spectra (S1b) of modified ZnO and shows its pattern according to ICDD number 30888, 30891, 50664, 211486, 471019 and
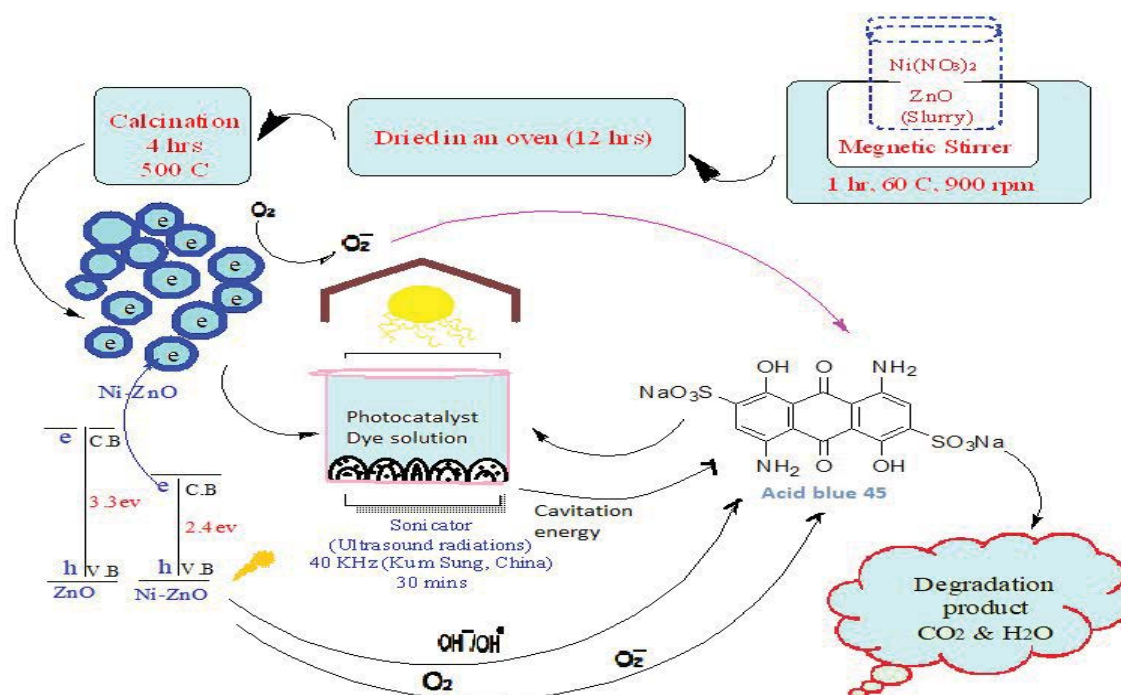


Fig. 1. The schematic diagram for the preparation of Ni–ZnO photocatalyst and degradation process.
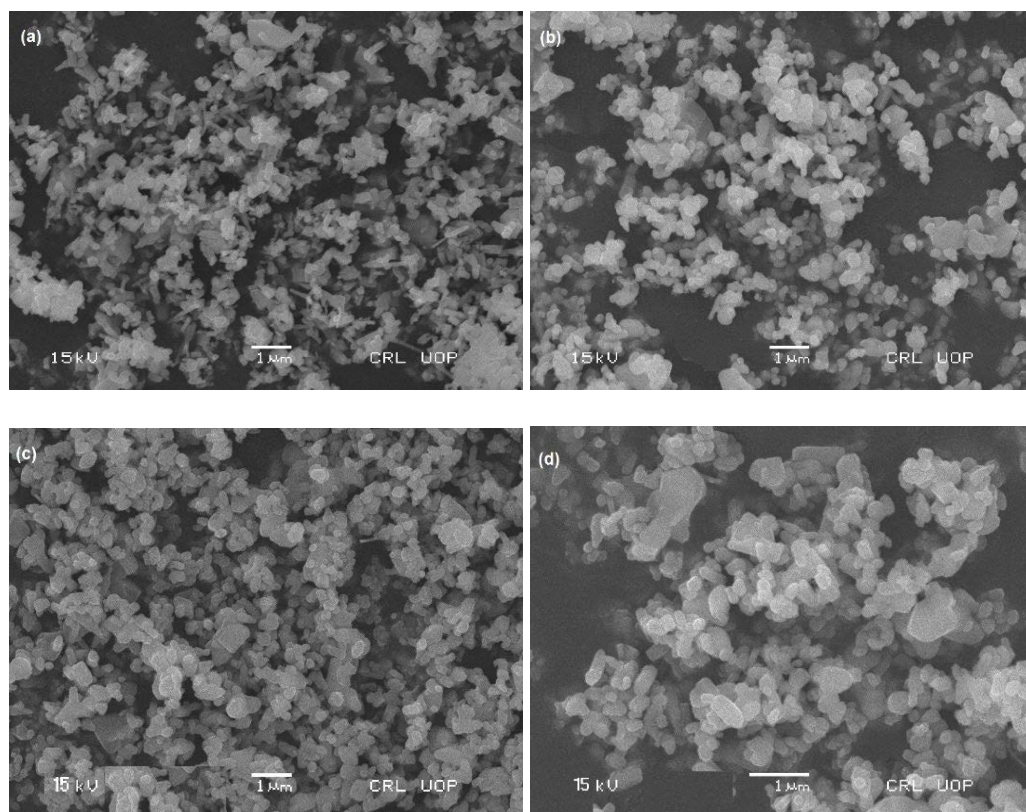
Fig. 2. SEM of (a) ZnO (b) Ni–ZnO, (c) fifth time re-used photocatalyst and (d) photocatalyst after washing.

11025. While spectra (S1c) is of five-time used Ni–ZnO, it shows the pattern at ICDD number 30891, 11136, 361451 and 471019 and spectra (S1d) is of re-used Ni–ZnO after washing shows ICDD 11136, 30891, 50664, 211486, 11238, 330989 and 380474. The ICCD numbers were found out with the help of XRD software. After impregnation of nickel on ZnO, the spectra of ZnO achieve the same XRD patterns except that peak intensities decreased because of the impregnation of nickel on the surface of ZnO. As $Ni^{2+}$ is comparatively smaller in atomic radius than $Zn^{2+}$ therefore no extra peaks were observed which indicated that no disturbance occurred in the wurtzite structure after nickel impregnation [15,16].

Peak height, area and its thickness were calculated using the Scherrer's equation (Tables S1.1, S1.2, S1.3, S1.4) for ZnO, Ni–ZnO, five times re-used Ni–ZnO and re-used Ni–ZnO after washing, it can easily observe that reflections range $2\theta$ values ranged from 28°–69°. The crystal lattice thickness measured by Scherrer's equation and suggests that thickness of crystal ranged from 17.8–44.8 nm in case of ZnO, 18.2 to 37.4 nm in case of Ni–ZnO and 19.8 to 38.1 nm for five-time re-used Ni–ZnO and 20.2 to 41.9 nm for re-used Ni–ZnO after washing. Bragg's law was applied to calculate the distance (d) between particle to particle and observed from 0.271 to 0.63 nm for all photocatalysts.

BET method was used for surface area determination and found that the ZnO surface area was 185.274 $m^2$ $g^{-1}$ and the surface area of Ni–ZnO was 180.88 $m^2$ $g^{-1}$. The results indicated that small change in the impregnated ZnO surface area is because of the impregnation of nickel on the ZnO surface.

The UV-visible spectrophotometric method was used for the optical properties determination of ZnO and Ni–ZnO (Figs. S2a and b). The plot of $(Ah\upsilon)^2$ vs. h$\upsilon$ (ev) was used for bandgap determination and equation $E_g$ = 1,240/wavelength ($\lambda$) was used for the energy of photon calculation. The bandgap energy after nickel impregnation shifted from UV (ZnO = 3.3 ev) to visible region (Ni–ZnO = 2.4 ev). The results revealed that the ZnO bandgap between the valence band and conduction band after impregnation with nickel decreased.

*3.2. Photocatalytic activity*

To confirm the change of conduction band of ZnO from UV to the visible region after nickel impregnation, the photocatalytic activity of ZnO and Ni–ZnO was compared under irradiation of UV and visible light. After impregnation with nickel (Ni–ZnO), the photocatalytic performance of ZnO has been shifted to the visible region (Fig. S3a).

Under different conditions such as adsorption, photolysis, photocatalysis, sonolysis, sonocatalysis and sonophotocatalysis the degradation of AV-49 and AB-45 were studied. The adsorption process results in a 0.5% dye adsorption on the Ni–ZnO photocatalyst. In the absence of photocatalyst, no dye degradation was found in the process of photolysis and sonolysis. However, degradation was observed in photocatalysis and sonocatalysis, which was further increased in the combined process of sonophotocatalysis (Fig. S3b). It may be explained by the mechanism of hot spots formation
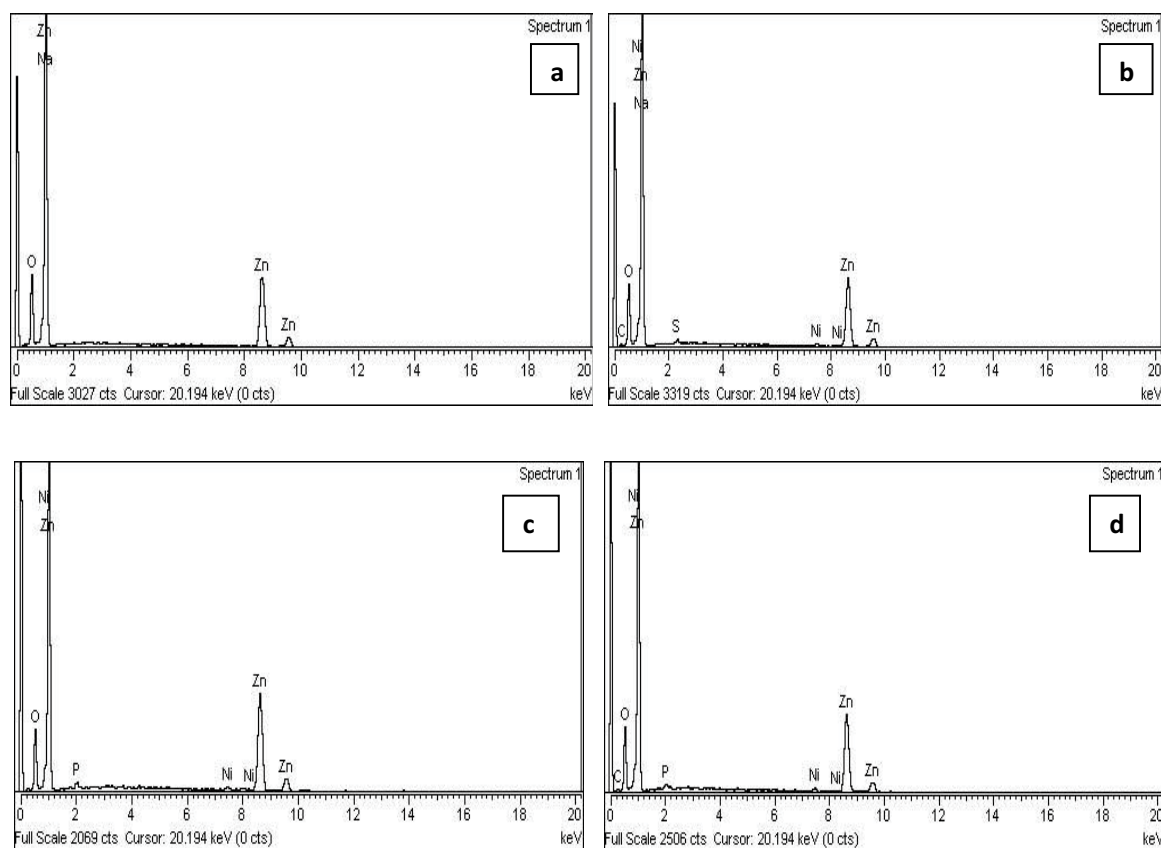
Fig. 3. EDX of (a) ZnO (b) Ni–ZnO, (c) re-used Ni–ZnO and (d) photocatalyst after washing.

and followed by sonoluminescence. First, the cavitation bubbles formed due to the heterogeneous nucleation of bubbles which generate hot spots in the solution. These hot spots then cause $H_2O$ molecules to disintegrate and form OH• radical. Second, sonoluminescence involves light, which excites the photocatalyst particles to act as photocatalysts during sonication. In the sonochemical reaction, the sonolysis of water as the solvent inside collapsing cavitation bubbles under extremely high temperature and pressure involves in the degradation of organic compounds (dyes). When a photocatalyst is added to the same solution, ultrasonic irradiation induces the sonolysis of water and photocatalyst produces electron-hole pairs. The electron-hole pairs produce OH• radicals and anions of superoxide •$O^{2-}$, which decomposes dyes to $CO_2$, $H_2O$, and inorganic species.

The photocatalytic degradation of dyes was also compared using irradiation source as sunlight and 200 W tungsten filament lamp. The data confirm the degradation efficiency of dyes in case of sunlight achieved (–89%) for the initial 60 min of exposure (compared to 200 W bulb (–91.6%) for the same time of exposure (Fig. S3c)).

### 3.3. pH effect

The pH effect on photocatalytic degradation of AV-49 and AB-45 was investigated from pH 2–10 (Fig. 4). AV-49 was degraded up to 11.1% and AB-45 up to 10.8% at pH 10. At alkaline pH, the surface of AV-49 and AB-45 becomes

negatively charge, which acts as strong nucleophiles. These strong nucleophiles will be very reactive towards the electrophilic attack of the OH• radicals. Alkaline pH also results in the increased formation of OH• radicals. At acidic pH, a decrease in the degradation of dyes may be because of a decline in the OH• radical concentration or may be due to protonation of amine group which become an electrophile and could not be attacked by another electrophile (OH• radicals). The same effect of pH 10 was observed by Zuorro et al. [17] in the degradation of reactive violet 5 dye.

### 3.4. Effect of oxidizing agents

Different oxidizing agents such as hydrogen peroxide ($H_2O_2$), sodium perchlorate ($NaClO_4$) and potassium peroxydisulphate ($K_2S_2O_8$) were studied as an enhancer for the sonophotocatalytic degradation of AV-49 and AB-45. As these oxidizing agents speed up the degradation process by the formation of more active free radicals therefore, they are also called enhancers. The increase in degradation efficiency is due to the increased production of OH• radicals. Oxidizing agents increase the rate of free radicals OH• production in two ways. Firstly, the reduction of oxidizing agent produces OH• radicals such as $H_2O_2$ at the conduction band. Secondly, the self decomposition as a result of ultrasonic waves also produces OH• radicals [3]. The results are presented in Fig. 5a for AB-45 and Fig. 5b for AV-49. The concentration of each oxidizing agent was varied
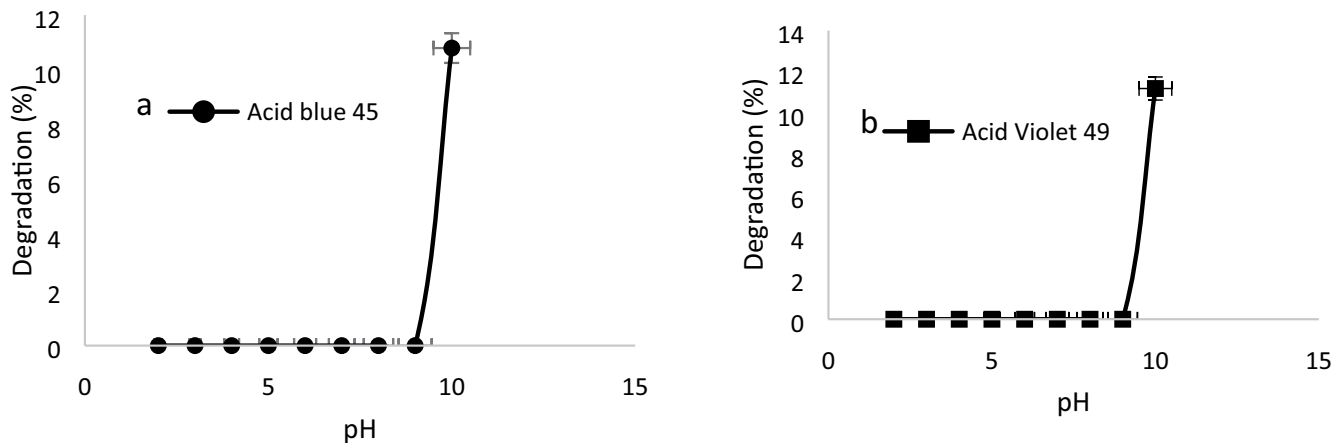
Fig. 4. Degradation of (a) Acid Blue 45 and (b) Acid Violet 49 using different pH.
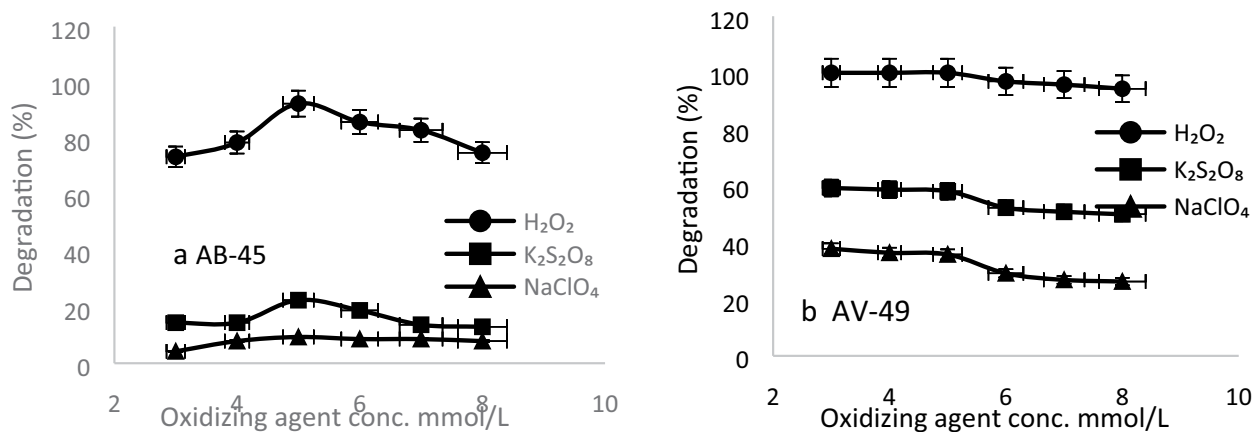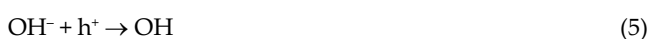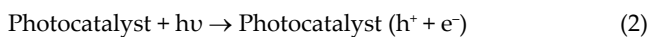


Fig. 5. Effect of oxidizing agents on the degradation of (a) Acid Blue 45 and (b) Acid Violet 49.

from 3 to 8 mmol and other conditions were kept constant (pH = 10, catalyst dose = 0.2 g L$^{-1}$ and dye initial concentration 10 mg L$^{-1}$). The sonophotocatalytic degradation of AV-49 increased from 11.9% to 100%, 37.8% and 59.3% with 5 mmol of hydrogen peroxide, 3 mmol of sodium perchlorate and 3 mmol of potassium peroxydisulfate, respectively. While the photocatalytic degradation AB-45 increased from 10.8% to 92.5%, 9.3% and 22.4% with 5 mmol of all three oxidizing agents. Reactions of the hydroxyl radicals are given in the following equations (Eqs. (2)–(8)) and the same degradation mechanism was also mentioned in literature [18–21].
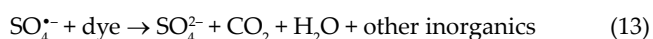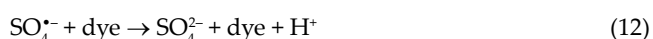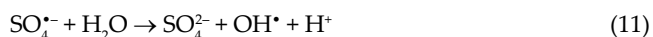
$$Photocatalyst + h\upsilon \rightarrow Photocatalyst\ (h^+ + e^-) \qquad (2)$$

$$H_2O_2 + h\upsilon/us \rightarrow OH^\bullet + H^+ \qquad (3)$$

$$H_2O + h\upsilon/us \rightarrow OH^- + H^+ \qquad (4)$$

$$OH^- + h^+ \rightarrow OH \qquad (5)$$

$$OH + Dye \rightarrow CO_2 + H_2O \qquad (6)$$

$$O_2 + e^- \rightarrow O_2 \qquad (7)$$

$$^\bullet O_2 + Dye \rightarrow CO_2 + H_2O \qquad (8)$$

As mentioned in Eq. (3), electromagnetic radiation and ultrasonic waves both produce OH$^\bullet$ radical. As well as the holes (h$^+$) produce from the interaction of electromagnetic radiation with photocatalyst (Eq. (2)) react with OH$^-$ ions produced from water due to sonophotolysis, Eq. (4) and results in the formation of $^\bullet$OH radical.

Sodium perchlorate effect on the degradation of AV-49 and AB-45 is due to capturing the electron generated on the conduction band of photocatalyst (Eq. (9)) [3].

$$ClO_4^- + 8e^- + 8H^+ \rightarrow Cl^- + 4H_2O \qquad (9)$$

Potassium peroxydisulphate as an oxidizing agent also increases the degradation of dyes due to the formation of sulfate radicals, which react with water and form OH$^\bullet$ radicals (Eqs. (10)–(13)) [20,21]. The synergistic effect of combining photocatalysis with sonolysis may be accredited to various reasons, increased production of hydroxyl radicals in the reaction mixture, enhanced mass transfer of dye molecules from the liquid phase to the surface of photocatalyst, photocatalyst excitation by ultrasound-induced luminescence

which has a wide wavelength range below 375 nm and increased photocatalytic activity due to de-aggregation of photocatalyst particles with the use of ultrasounds which increased surface area [22,23].

$$S_2O_8^{2-} + h\upsilon \rightarrow 2SO_4^{\bullet-} \tag{10}$$

$$SO_4^{\bullet-} + H_2O \rightarrow SO_4^{2-} + OH^{\bullet} + H^+ \tag{11}$$

$$SO_4^{\bullet-} + dye \rightarrow SO_4^{2-} + dye + H^+ \tag{12}$$

$$SO_4^{\bullet-} + dye \rightarrow SO_4^{2-} + CO_2 + H_2O + other\ inorganics \tag{13}$$

It was found that maximum degradation was achieved in the presence of $H_2O_2$ (5 mmol) at pH 10 due to the increased production of hydroxyl radicals which increased the rate of degradation (Eq. (6)). Above 5 mmol, hydroxyl radicals reacted with $H_2O_2$ and produced $HO_2^{\bullet}$ (Eq. (14)). $HO_2^{\bullet}$ radicals are less reactive than $OH^{\bullet}$ radicals and therefore retard the degradation at higher concentrations of $H_2O_2$.

$$H_2O_2 + OH^{\bullet} \rightarrow HO_2^{\bullet} + H_2O \tag{14}$$

The rate of degradation of both dyes with $H_2O_2$ was greater as compared to other oxidizing agents and further study was carried out with 5 mmol of $H_2O_2$ for AV-49 and AB-45.

### 3.5. Photocatalyst loading effect

The effect of photocatalyst amount on the degradation of AV-49 and AB-45 was studied to improve the cost efficiency of the sonophotocatalytic degradation process. The amount of photocatalyst was varied in the range of 0.01–0.35 g $L^{-1}$ at pH 10 using 10 mg $L^{-1}$ concentration of AV-49/AB-45 and 5 mmol of $H_2O_2$ (Fig. 6a). It was found that with a very small quantity of photocatalyst, that is, 0.01 g $L^{-1}$ of Ni–ZnO gives 100% degradation with AV-49 and with an increase in the amount of photocatalyst (0.01–0.1 g $L^{-1}$) there

was an increase in degradation of AB-45 dye. Maximum degradation of AV-49 and AB-45 was found 100% with 0.01 g $L^{-1}$ and 92.5% with 0.1 g $L^{-1}$ dose of photocatalyst, respectively. Further increase in the amount of photocatalyst leads to an insignificant decrease in the degradation of AB-45 dye. It may be due to photocatalyst particle aggregation which results in decreasing the active points of the photocatalyst for $OH^{\bullet}$ radical generation. As well as the excess amount of photocatalyst results in light scattering and in turn reduce the rate of the degradation process. Moreover, it is also involved in the reduction of solution transparency which prevents radiation penetration.

### 3.6. Effect of dye concentration

The initial concentration effect of AV-49 and AB-45 was studied on sonophotocatalytic degradation in the range of 10 to 100 mg $L^{-1}$. It was found that by applying ultrasonic waves for 10 mg $mL^{-1}$ of AV-49 with 0.01 g of Ni–ZnO, pH 10 and 5 mmol of $H_2O_2$, 100% degradation of AV-49 was achieved in 20 min (Fig. 6b). While in the case of 10 mg $L^{-1}$ of AB-45 with 0.2 g of Ni–ZnO, pH 10 and 5 mmol of $H_2O_2$, 100% degradation was also achieved in 20 min (Fig. 6). As shown in Fig. 6b, the photocatalyst efficiency decreased slowly with an increase in AV-49 and AB-45 initial concentration. AV-49 of 100 mg $L^{-1}$ was degraded 94.1% in 60 min while 100 mg $L^{-1}$ of AB-45 was degraded 35.6% in 60 min. It may be due to a decrease in $OH^{\bullet}$ radical concentration with an increase in dye concentration. It was found that with an increase in photocatalyst amount, percentage of dye degradation was also increased, 94.1% degradation was achieved with 0.01 g $L^{-1}$ of Ni–ZnO, while 95.1% with 0.05 g $L^{-1}$ of Ni–ZnO and 97.4% with 0.1 g $L^{-1}$ of Ni–ZnO in 60 min using AV-49 dye (Figs. S4a, b and S5).

### 3.7. Effect of scavengers

Keeping in mind the application of the method for environmental samples, the effect of scavengers was also studied. As natural effluent samples of textile/dyeing
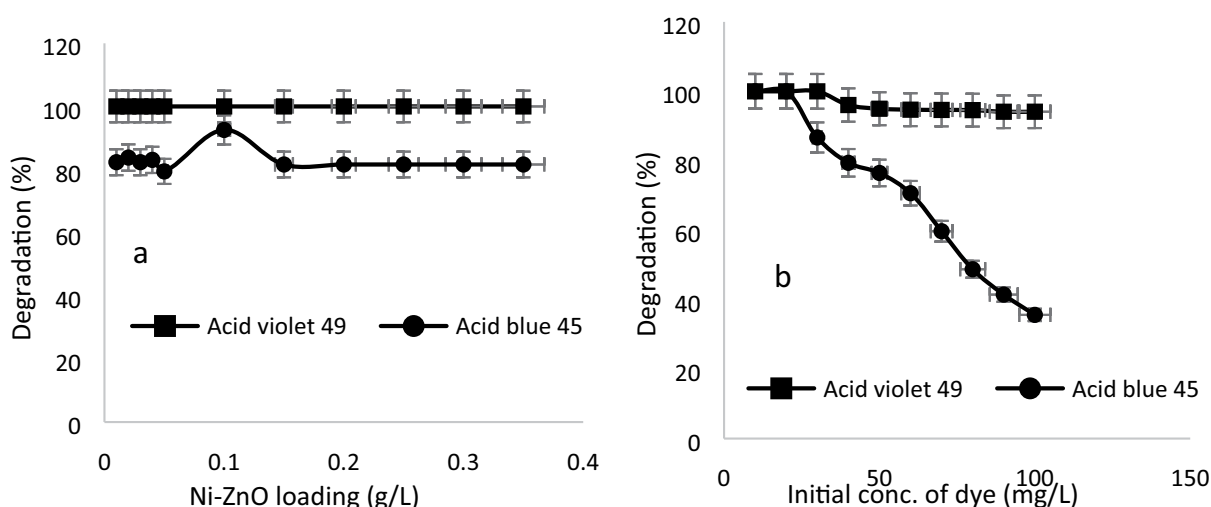


Fig. 6. Effect of (a) photocatalyst amount and (b) initial concentration of dye on degradation.
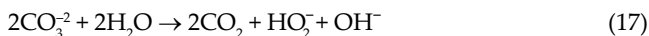
industries contain anions such as $Cl^-$, $SO_4^{-2}$, $CO_3^{-2}$, $PO_4^{3-}$, $BrO_3^-$, $HCO_3^-$ therefore, the effect of these anions was investigated for both dyes. It was observed that these anions decrease the efficiency of sonophotocatalytic degradation because these anions trap the formation of free oxidizing radicals and react with $OH^\bullet$ radical [24,25]. The scavengers studied in the present study were chlorides, sulfates and carbonates.

In a scavenger study, first the effect of chloride was investigated for AV-49 and AB-45 dyes. Keeping all the conditions constant and different concentrations of chloride in the range of 0.025–0.15 M was used in sonophotocatalytic degradation.

It was found that it increases the degradation time of AV-49 from 100% degradation in 20 to 60 min (Fig. 7a), in case of AB-45 it affected the degradation of dye and decreased the degradation from 100% in 20 min to 68.4% in 60 min (Fig. 7b). The possible reaction that may occur is shown in the equation (Eq. (15)) [24,25].

$$Cl^- + OH^\bullet \rightarrow Cl^\bullet + OH^- \tag{15}$$

Effect of different concentrations of carbonate in the range of 0.025–0.15 M on the degradation of AV-49 and AB-45 was studied. It was found that in case of AV-49 degradation of dye from 100% in 20 min was slowed down to 100% in 40 min (Fig. 7a) and in case of AB-45 degradation was slowed down from 100% in 20 min to 91% in 60 min (Fig. 7b). The possible reaction is given in the following equations (Eqs. (16)–(18)) [26,27].

$$CO_3^{-2} + OH^\bullet \rightarrow CO_3^{\bullet-} + OH^- \tag{16}$$

$$2CO_3^{-2} + 2H_2O \rightarrow 2CO_2 + HO_2^- + OH^- \tag{17}$$

$$OOH^- + OH^\bullet \rightarrow OH^- + OOH \tag{18}$$

The oxidation potential of the generated radical anion ($CO_3^{\bullet-}$) is lower than the hydroxyl radical therefore the active sites on the surface of Ni–ZnO photocatalyst may be blocked by the carbonate anions which leads to the deactivation of the photocatalyst towards the dye.

Effect of sulfate anion as a scavenger was also studied for both dyes. It was found that 0.1 M concentration of sulfates increased the degradation time from 20 to 30 min for 100% degraded of AV-49 (Fig. 7a) and in case of AB-45, degradation process decreased to 23.2% in 60 min (Fig. 7b). A possible reaction is given in Eq. (19) [21].

$$SO_4^{-2} + OH^\bullet \rightarrow SO_4^{\bullet-} + OH^- \tag{19}$$

The presence of all three studied scavengers in the solutions of dye caused a decrease in the degradation efficiency of AV-49 and AB-45 which confirmed that the dominant controlling mechanism for sonophotocatalytic degradation is the attack of free radical.

The studied anions are known to interact with the reactive $OH^\bullet$ radical and deactivate them. The anions can also get adsorbed on the surface of photocatalyst and block the surface sites from adsorption by the substrates and inhibit the reactive species formation [22].

*3.8. Photocatalyst re-usability*

The photocatalyst re-usability is important to assess its practical use. For re-usability, the sonophotocatalytic activity of Ni–ZnO photocatalyst was studied. After degradation of dye, the photocatalyst was collected through centrifugation and washed with different polar organic solvents (ethanol, methanol, acetone and acetonitrile) and then with distilled water. The effect of the solvents used for washing of photocatalyst was the same due to the solubility of the adsorbed dye in organic solvents. Therefore, ethanol was selected from cost, availability and safety of view for further washing of photocatalyst. After drying the photocatalyst was used again with fresh dye solution at the optimized conditions of degradation. The photocatalyst was run for five cycles, it was found that in case of AV-49 the degradation of dye decreased to 88.5% and increased the degradation time by using again and again (Fig. S5a). The reusability of photocatalyst for AB-45 was also checked and found that at the fifth run the AB-45 was 34.8% degraded in 60 min (Fig. S5a). The decrease in the activity of the photocatalyst may be due to the adsorption of intermediate compounds on the surface of photocatalyst.

Keeping in mind its commercial application the settling time of photocatalyst was also studied. It was found that for 0.2 g $L^{-1}$ photocatalyst settling time was 154 min while



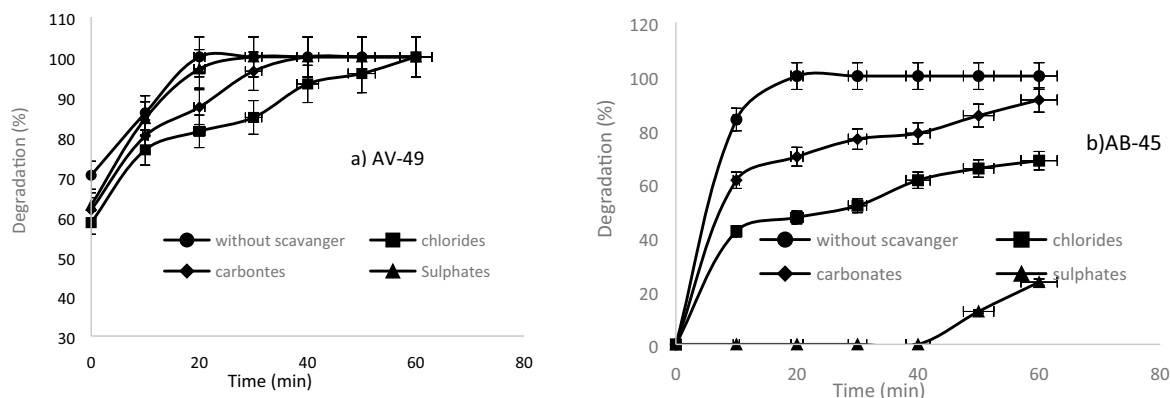Fig. 7. Effect of different types of scavengers on the degradation of (a) Acid Violet 49 and (b) Acid Blue 45.

for 0.05 g L⁻¹ was 60 min. An increase in the photocatalyst amount increased the time for the settling of photocatalyst (Fig. S6).

### 3.9. Sample application

The proposed sonophotocatalytic method for the degradation of textile dyes was applied to two different samples of water. One sample was collected from wastewater of small-scale fabric dyeing industry and the second was prepared synthetically. The sonophotocatalytic degradation of the samples was carried out at optimum conditions of pH, $H_2O_2$, photocatalyst amount and degradation was calculated. It was observed that the synthetic sample was degraded 92.3% at optimum conditions and the industrial sample was degraded 88.5% in 60 min (Fig. 8). A decrease in the degradation of industrial samples is due to the presence of different anions acting as scavengers.

### 3.10. Kinetic of AV-49 and AB-45 degradation

The kinetics of the sonophotocatalytic degradation of AV-49 and AB-45 dyes was performed and the rate constants were determined by the different kinetic models. The pseudo-first-order kinetic and pseudo-second-order linear forms of equations are as follows:

$$\log\left(q_e - q_t\right) = \log q_e - \frac{k_1 t}{2.303} \tag{20}$$

$$\frac{t}{q_t} = \frac{1}{K_2 q_t^2} + \frac{t}{q_e} \tag{21}$$

where $q_e$ and $q_t$ are the amounts of dye degraded (mg g⁻¹) at equilibrium and at any given time (min) while $K_1$ and $K_2$ are the rate constant for pseudo-first-order and pseudo-second-order kinetic models. A plot of $\log (q_e - q_t)$ vs. $t$ illustrated in Fig. 9. The sonophotocatalytic degradation of AV-49 and AB-45 followed the pseudo-first-order kinetic model as its $R^2$ value is greater than the pseudo-second-order kinetic model and $q_e$ experimental value is also close to the $q_e$

value of the pseudo-first-order kinetic model. The rate of degradation of AV-49 is higher ($K_1$ = 0.044) than the AB-45 ($K_1$ = 0.040). A comparison of the kinetic data for both dyes is given in Table S2.

### 3.11. Mechanism of degradation

The organic compounds (dyes) degradation using sonophotocatalytic process occurs in various parts of the aqueous solution: (a) bulk solution, (b) interface between the bulk solution and cavitation bubbles, (c) interface between the particles of photocatalyst and cavitation bubbles, and (d) inside the cavitation bubbles. In the cavitation bubble and interface of the cavitation bubble with bulk solution mainly the OH• radical formation occurs. While in the bulk solution at the cavitation interface with a photocatalyst, OH• radicals with dye molecules, transfer of electron (e⁻) directly from the surface of Ni–ZnO photocatalyst to the dye molecules as well as direct reaction with holes (h+). The hydrophilic compounds are mainly degraded through the OH• radical reaction at the interface of cavitation and bulk solution. The impregnation of nickel on ZnO photocatalyst also enhanced the adsorption of organic dye on the photocatalyst surface which results in increased interaction of dye molecules with OH• radical. The degradation process through OH• radical was also confirmed by the addition of OH• radical scavengers and a decrease in degradation efficiency was observed. The possible degradation mechanism is AV-49 is shown in Fig. 10.

### 3.12. Comparison with other methods of removal

The proposed sonophotocatalytic degradation method for AV-49 and AB-45 dyes using Ni–ZnO photocatalyst was compared with other degradation methods but it was found that in the literature there is no reported method for the degradation of AV-49. While degradation of AB-45 using different photocatalysts and sources of irradiation were found in the literature and are shown in Table 1. It can be concluded that the proposed sonophotocatalytic degradation method using Ni–ZnO photocatalyst is superior as compared to the reported methods.
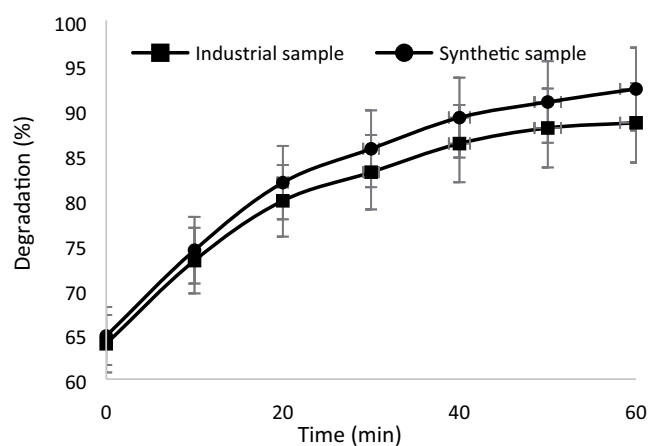


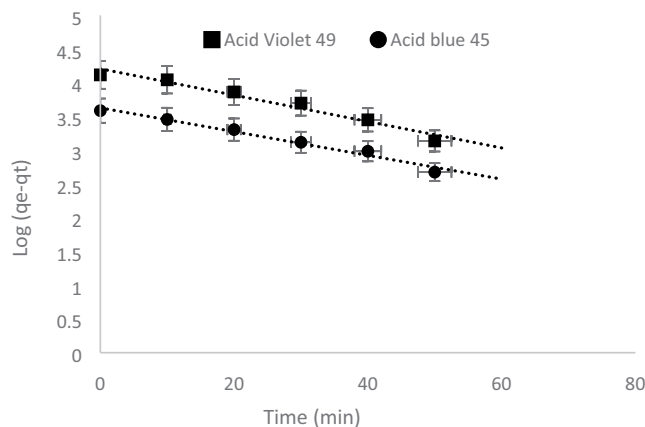Fig. 8. Degradation of the sample at optimum conditions.



Fig. 9. Pseudo-first-order kinetic model for Acid Violet 49 and Acid Blue 45.
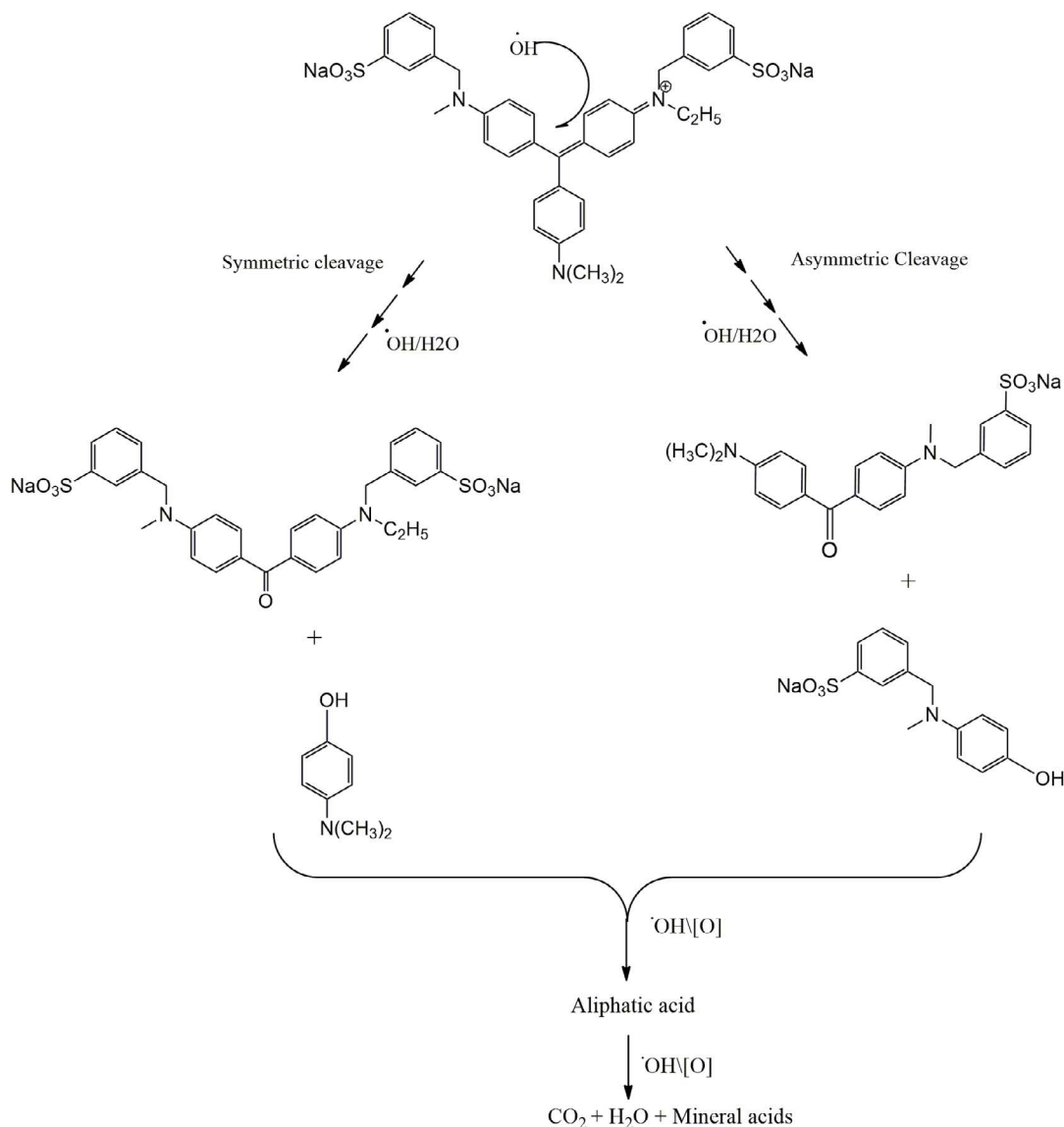
Fig. 10. Proposed degradation mechanism of Acid Violet 49.

Table 1
Comparison of the proposed degradation method with reported degradation methods for Acid Violet 49 and Acid Blue 45

| No. | Dye | Degradation source | Catalyst | Time | % Degradation | References |
|-----|-----|--------------------|----------|------|---------------|-----------|
| 1 | Acid Blue 45 | 125 W Hg lamp | $TiO_2$ Hombikat UV100 | 80 min | 80%–90% | [25] |
| 2 | Acid Blue 45 | Novel open fungal reactor system | Ozone as a bactericide | 25 d | 84% | [28] |
| 3 | Acid Violet 49 | Ultrasonic waves with tungsten lamp (100 W) | Ni–ZnO | 20 min | 100% | Present work |
| 4 | Acid Blue 45 | Ultrasonic waves with tungsten lamp (100 W) | Ni–ZnO | 20 min | 100% | Present work |

## 4. Conclusion

Nickle impregnated zinc oxide (Ni–ZnO) photocatalyst was prepared via a wet impregnation method to improve the ability of ZnO to absorb longer wavelength radiations of visible light. Prepared photocatalyst was characterized by spectroscopic techniques like SEM, EDX, XRD and UV-visible. The results showed successful impregnation of nickel onto the ZnO surface. The degradation of two acidic dyes, AV-49 and AB-45, were investigated in the

presence of Ni–ZnO photocatalyst. Results revealed an increase in degradation process under visible light in the presence of ultrasonic waves. Ultrasonic waves increased the number of oxidizing radicals due to cavitation energy which is responsible for the degradation process. The pseudo-first-order rate constants are $K_1$ = 0.044 and $K_1$ = 0.040 for the sonophotocatalytic degradation of AV-49 and AB-45, respectively. It may be concluded that Ni–ZnO photocatalyst is a good photocatalyst for the treatment of textile and dyeing industries effluents.

## Acknowledgment

## References

[1] X. Zhou, Y.Z. Li, T. Peng, W. Xie, X.J. Zhao, Synthesis, characterization and its visible-light-induced photocatalytic property of carbon doped ZnO, Mater. Lett., 63 (2009) 1747–1749.

[2] M. Ahmad, E. Ahmed, Y. Zhang, N.R. Khalid, J. Xu, M. Ullah, Z. Hong, Preparation of highly efficient Al-doped ZnO photocatalyst by combustion synthesis, Curr. Appl. Phys., 13 (2013) 697–704.

[3] A. Khataee, A. Karimi, S. Arefi-Oskoui, R.D.C. Soltani, Y. Hanifehpour, B. Soltani, S.J. Joo, Sonochemical synthesis of Pr-doped ZnO nanoparticles for sonocatalytic degradation of Acid Red 17, Ultrason. Sonochem., 22 (2015) 371–381.

[4] J. Shah, M.R. Jan, F. Khitab, Sonophotocatalytic degradation of textile dyes over Cu impregnated ZnO catalyst in aqueous solution, Process Saf. Environ. Prot., 116 (2018) 149–158.

[5] F. Khitab, M.R. Jan, J. Shah, Sonophotocatalytic degradation of aqueous Acid Red 27 and Direct Violet 51 using copper impregnated $Al_2O_3$, Desal. Water Treat., 137 (2019) 381–394.

[6] M. Mahendiran, J.J. Mathen, M. Racik, J. Madhavan, M.V.A. Raj, Investigation of structural, optical and electrical properties of transition metal oxide semiconductor CdO-ZnO nanocomposite and its effective role in the removal of water contaminants, J. Phys. Chem. Solids, 126 (2019) 322–334.

[7] A. Phuruangrat, S. Siri, P. Wadbua, S. Thongtem, T. Thongtem, Microwave-assisted synthesis, photocatalysis and antibacterial activity of Ag nanoparticles supported on ZnO flowers, J. Phys. Chem. Solids, 126 (2019) 170–177.

[8] R. Saravanan, S. Karthikeyan, V.K. Gupta, G. Sekaran, V. Narayanan, A. Stephen, Enhanced photocatalytic activity of ZnO/CuO nanocomposite for the degradation of textile dye on visible light illumination, Mater. Sci. Eng., C, 33 (2019) 91–98.

[9] Z.M. He, Y.M. Xia, B. Tang, J.B. Su, X.F. Jiang, Optimal co-catalytic effect of $NiFe_2O_4$/ZnO nanocomposites towards enhanced photodegradation for dye MB, Z. Phys. Chem., 233 (2019) 347–359.

[10] M. Saeed, M. Siddique, M. Usman, A. Ulhaq, S.G. Khan, H.A. Raoof, Synthesis and characterization of zinc oxide and evaluation of its catalytic activities for oxidative degradation of rhodamine B dye in aqueous medium, Z. Phys. Chem., 231 (2017) 1559–1572.

[11] G. Madhumitha, J. Fowsiya, N. Gupta, A. Kumar, M. Sing, Green synthesis, characterization and antifungal and photocatalytic activity of *Pithecellobium dulce* peel–mediated ZnO nanoparticles, J. Phys. Chem. Solids, 127 (2019) 43–51.

[12] R.D.C. Soltani, S. Jorfi, H. Tamezani, S. Purfadakari, Ultra-sonically induced ZnO–biosilica nanocomposite for degradation of a textile dye in aqueous phase, Ultrason. Sonochem., 28 (2016) 69–78.

[13] H.T.S. Britton, Hydrogen Ions, E.H. Tripp, Ed., Monographs on Applied Chemistry, Chapman & Hall, Ltd., New York, NY, 1943, p. 313.

[14] Adnan, J. Shah, M.R. Jan, Polystyrene degradation studies using Cu supported catalysts, J. Anal. Appl. Pyrolysis, 109 (2014) 196–204.

[15] A. Bokare, M. Pai, A.A. Athawale, Surface modified Nd doped $TiO_2$ nanoparticles as photocatalysts in UV and solar light irradiation, Sol. Energy, 91 (2013) 111–119.

[16] N. Ertugay, F.N. Acar, The degradation of direct blue 71 by sono, photo and sonophotocatalytic oxidation in the presence of ZnO nanocatalyst, Appl. Surf. Sci., 318 (2014) 121–126.

[17] A. Zuorro, R. Lavecchia, M.M. Monaco, G. Iervolino, V. Vaiano, Photocatalytic degradation of azo dye reactive violet 5 on Fe-doped titania catalysts under visible light irradiation, Catalysis, 9 (2019) 645–651.

[18] P. Singh, M.C. Vishnu, K.K. Sharma, R. Singh, S. Madhav, D. Tiwary, P.K. Mishra, Comparative study of dye degradation using $TiO_2$-activated carbon nanocomposites as catalysts in photocatalytic, sonocatalytic, and photosonocatalytic reactor, Desal. Water Treat., 3994 (2015) 1–13.

[19] S. Tangestaninejad, M. Moghadam, V. Mirkhani, I. Moham-madpoor-Baltork, H. Salavati, Sonochemical and visible light induced photochemical and sonophotochemical degradation of dyes catalyzed by recoverable vanadium-containing polyphosphomolybdate immobilized on $TiO_2$ nanoparticles, Ultrason. Sonochem., 15 (2008) 815–822.

[20] U.I. Gaya, A.H. Abdullah, Heterogeneous photocatalytic degradation of organic contaminants over titanium dioxide: a review of fundamentals, progress and problems, J. Photochem. Photobiol., C, 9 (2008) 1–12.

[21] M. Qamar, M. Saquib, M. Muneer, Photocatalytic degradation of two selected dye derivatives, chromotrope 2B and Amido black 10B, in aqueous suspensions of titanium dioxide, Dyes Pigm., 65 (2005) 1–9.

[22] B. Rajeev, S. Yesodharan, E.P. Yesodharan, Sunlight activated ZnO mediated photocatalytic degradation of acetophenone in water, IOSR J. Appl. Chem., 1 (2016) 55–70.

[23] C. Lops, A. Ancona, K. Di Cesare, B. Dumontel, N. Garino, G. Canavese, S. Hérnandez, V. Cauda, Sonophotocatalytic degradation mechanisms of Rhodamine B dye via radicals generation by micro- and nano-particles of ZnO, Appl. Catal., B, 243 (2019) 629–640.

[24] M.A. Rauf, S.S. Ashraf, Fundamental principles and application of heterogeneous photocatalytic degradation of dyes in solution, Chem. Eng. J., 151 (2009) 10–18.

[25] M.A. Behnajady, N. Modirshahla, M. Shokri, Photodestruction of Acid orange 7 (AO7) in aqueous solutions by UV/$H_2O_2$: influence of operational parameters, Chemosphere, 55 (2004) 129–134.

[26] J. Shah, M.R. Jan, F. Khitab, Evaluation of magnetic nanoparticles as photocatalyst for the catalytic treatment of Direct red 28 dye in synthetic and real water effluents, Part. Sci. Technol., 36 (2018) 534–540.

[27] S. Kumawat, K. Meghwal, S. Kumar, R. Ameta, C. Ameta, Kinetics of sonophotocatalytic degradation of an anionic dye nigrosine with doped and undoped zinc oxide, Water Sci. Technol., 80 (2019) 1466–1475.

[28] M.A. Tariq, M. Faisal, M. Saquib, M. Muneer, Heterogeneous photocatalytic degradation of an anthraquinone and a triphenylmethane dye derivative in aqueous suspensions of semiconductor, Dyes Pigm., 76 (2008) 358–365.

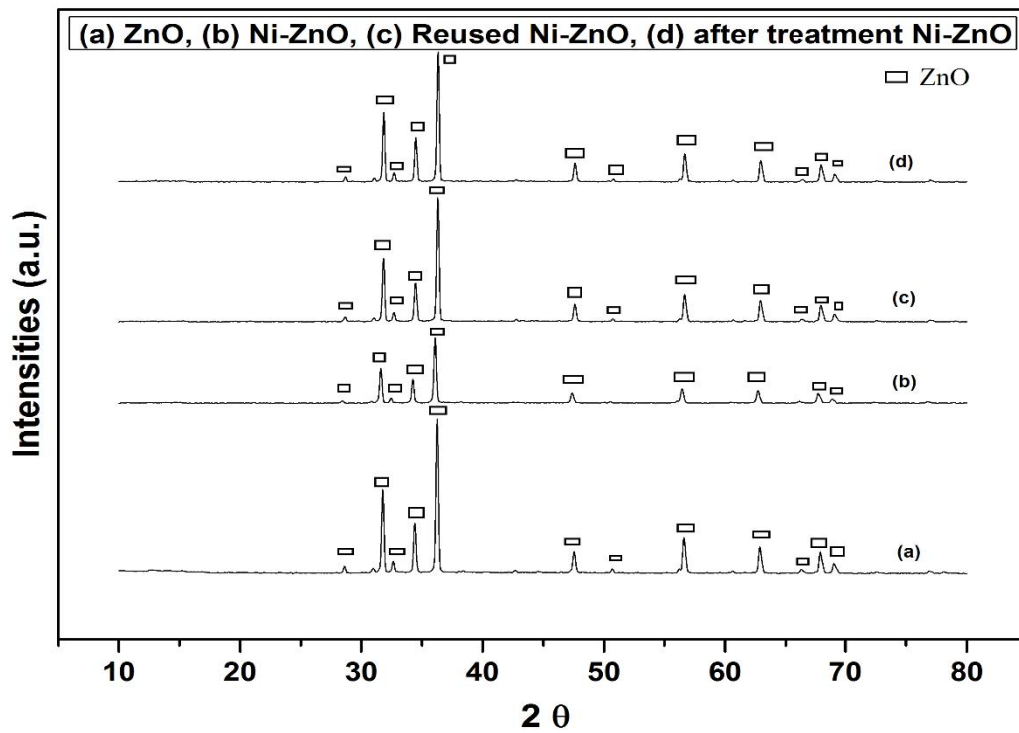**Supplementary information**



Fig. S1. XRD pattern of (a) ZnO, (b) Ni–ZnO, (c) after five-time re-used Ni–ZnO and (d) photocatalyst after washing.
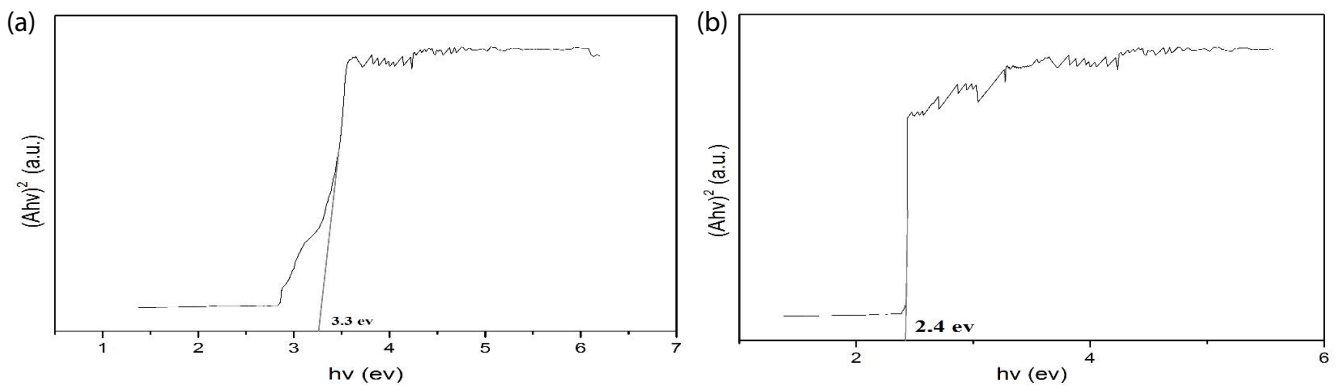


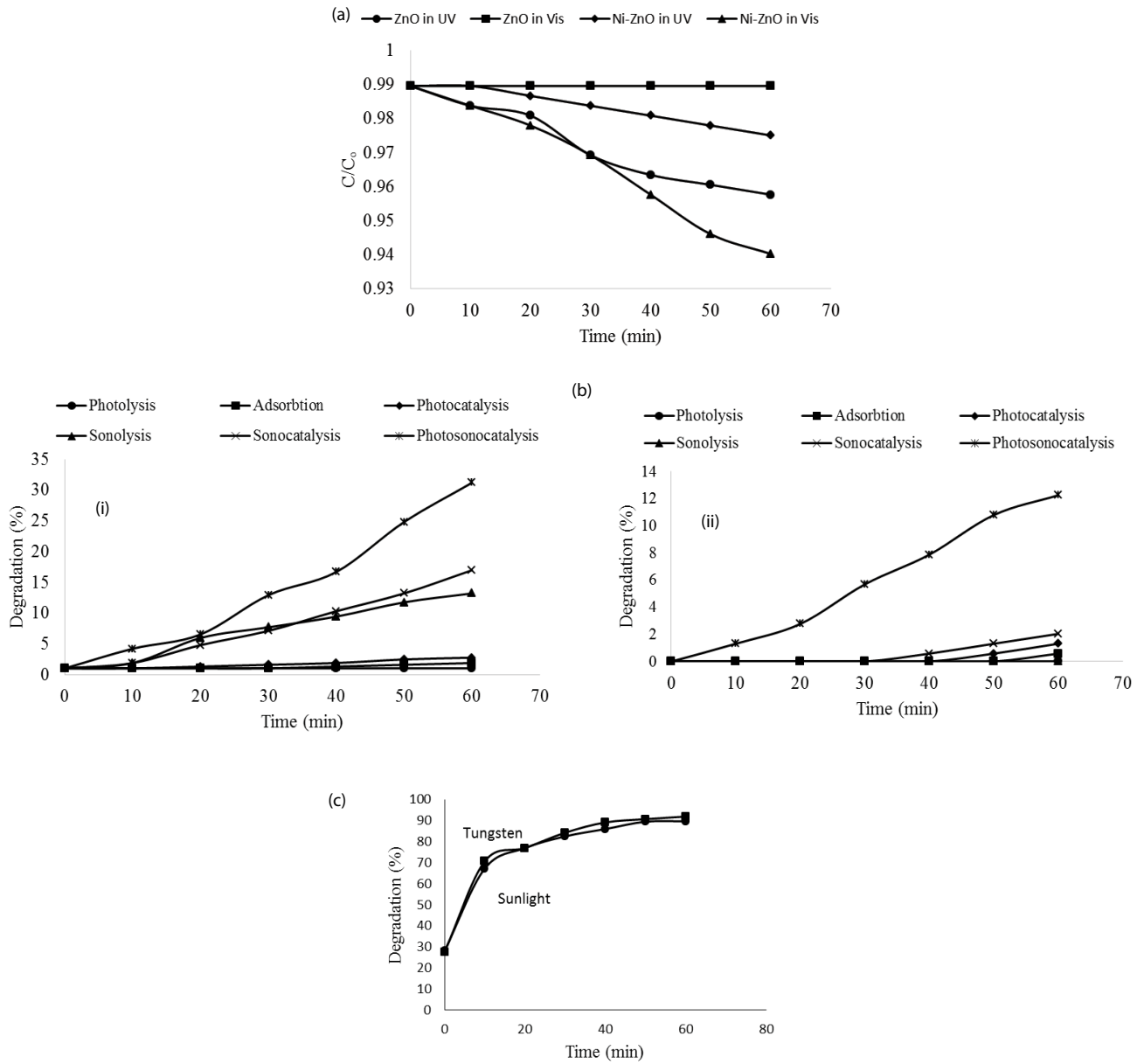Fig. S2. (a) Tauc plot for ZnO and (b) Ni–ZnO.

Fig. S3. (a) The absorbance of ZnO and Ni–ZnO under UV and visible light sources, (b) degradation of (i) Acid Violet 49 and (ii) Acid Blue 45 under different conditions at a different time (min), and (c) degradation of Acid Violet 49 tungsten lamp and sunlight under optimum conditions.
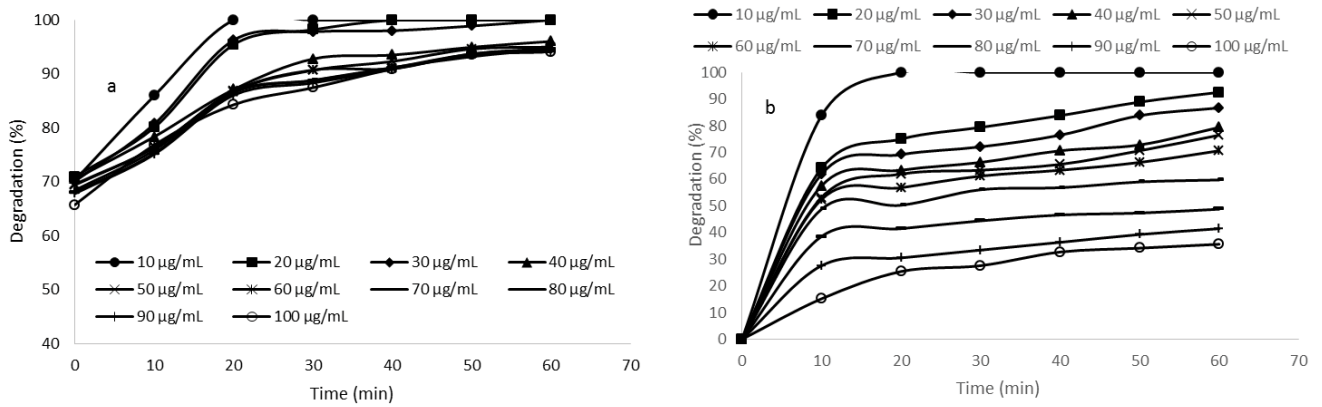
Fig. S4. Degradation of (a) Acid Violet 49 and (b) Acid Blue 45 at different initial concentrations.
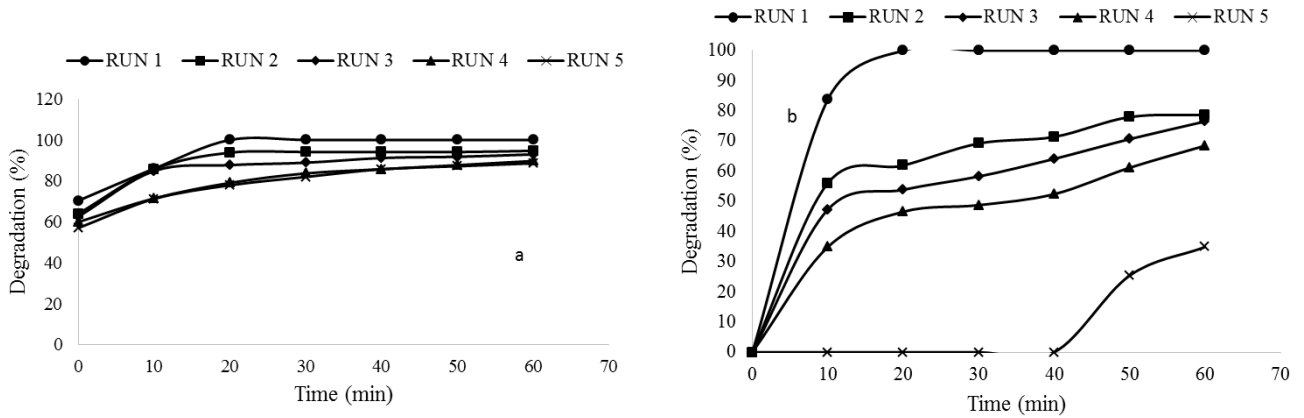


Fig. S5. Degradation of reusability of Ni–ZnO using (a) Acid Violet 49 and (b) Acid Blue 45. Reusability of Ni–ZnO.
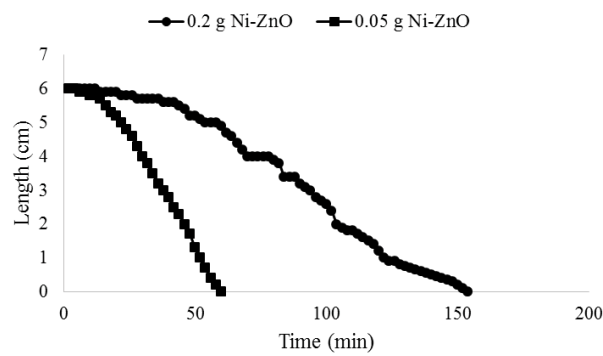


Fig. S6. Catalyst settling time.

Table S1.1
X-ray diffraction data for ZnO

| $2\theta$ | Height from base | Width (at half height) | Area | Thickness (nm) | Bragg's law |
|---|---|---|---|---|---|
| 28 | 295.7 | 0.003098 | 55.87795 | 44.87743 | 0.636819 |
| 31 | 3,150 | 0.003399 | 709.4 | 40.62334 | 0.576491 |
| 32 | 166.375 | 0.007735 | 3,296.17 | 17.80451 | 0.558924 |
| 34 | 2,215 | 0.003536 | 538.725 | 38.75043 | 0.526933 |
| 36 | 7,055 | 0.00319 | 1,563.55 | 42.71223 | 0.49855 |
| 47 | 853.880 | 0.003986 | 207.59 | 32.96249 | 0.386359 |
| 50 | 172.233 | 0.003143 | 33.018 | 41.3129 | 0.364538 |
| 56 | 1,537 | 0.004615 | 476.825 | 27.40891 | 0.328157 |
| 62 | 1,032.85 | 0.004628 | 291.619 | 26.53342 | 0.299124 |
| 66 | 137.73 | 0.005023 | 42.193 | 23.9231 | 0.282866 |
| 67 | 799.594 | 0.004946 | 241.288 | 24.15509 | 0.279126 |
| 69 | 354.362 | 0.005463 | 118.1712 | 21.61482 | 0.271996 |

Table S1.2
X-ray diffraction data for Ni–ZnO

| $2\theta$ | Height from base | Width (at half height) | Area | Thickness (nm) | Bragg's law |
|---|---|---|---|---|---|
| 28 | 92.48566 | 0.003716 | 20.96115 | 37.40981 | 0.636819 |
| 31 | 1,348.51729 | 0.003895 | 320.36457 | 35.44486 | 0.576491 |
| 32 | 188.31332 | 0.003683 | 42.30521 | 37.3899 | 0.558924 |
| 34 | 930.4217 | 0.003856 | 218.83866 | 35.52882 | 0.526933 |
| 36 | 919.04675 | 0.003784 | 212.08585 | 36.01351 | 0.49855 |
| 47 | 2,574.35948 | 0.003951 | 620.32443 | 33.25663 | 0.386359 |
| 50 | 387.79326 | 0.004841 | 114.50294 | 26.82159 | 0.364538 |
| 56 | 519.38877 | 0.004665 | 147.79496 | 27.11464 | 0.328157 |
| 62 | 472.15862 | 0.005178 | 149.11816 | 23.71642 | 0.299124 |
| 66 | 55.34249 | 0.005946 | 20.06888 | 20.20967 | 0.282866 |
| 67 | 364.21651 | 0.00593 | 131.72875 | 20.14761 | 0.279126 |
| 69 | 171.07526 | 0.006478 | 67.59744 | 18.22586 | 0.271996 |

Table S1.3
X-ray diffraction data for reused Ni–ZnO

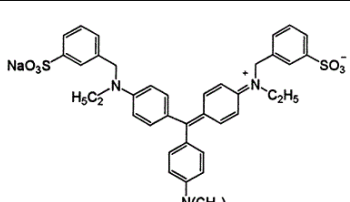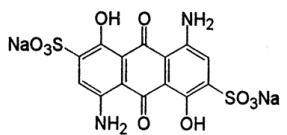| $2\theta$ | Height from base | Width (at half height) | Area | Thickness (nm) | Bragg's law |
|---|---|---|---|---|---|
| 28 | 175.91944 | 0.003937 | 42.24028 | 35.31186 | 0.636819 |
| 31 | 2,565.84214 | 0.003777 | 591.08546 | 36.552 | 0.576491 |
| 32 | 334.40428 | 0.003612 | 73.67731 | 38.12513 | 0.558924 |
| 34 | 1,531.60374 | 0.003965 | 370.36845 | 34.55759 | 0.526933 |
| 36 | 4,965.90239 | 0.003816 | 1,155.67451 | 35.71041 | 0.49855 |
| 47 | 674.24257 | 0.004283 | 176.14605 | 30.67393 | 0.386359 |
| 50 | 94.90964 | 0.003654 | 21.15469 | 35.53198 | 0.364538 |
| 56 | 1,035.70967 | 0.004674 | 295.27503 | 27.06301 | 0.328157 |
| 62 | 818.54802 | 0.005176 | 258.38876 | 23.72842 | 0.299124 |
| 66 | 92.51782 | 0.006041 | 34.08838 | 19.8903 | 0.282866 |
| 67 | 621.42381 | 0.005312 | 201.33179 | 22.49163 | 0.279126 |
| 69 | 275.50946 | 0.005575 | 93.68357 | 21.17906 | 0.271996 |

Table S1.4
X-ray diffraction data for reused Ni–ZnO after treatment

| $2\theta$ | Height from base | Width (at half height) | Area | Thickness (nm) | Bragg's law |
|---|---|---|---|---|---|
| 28 | 194.87015 | 0.003436 | 40.84008 | 40.45762 | 0.636819 |
| 31 | 2.745.73681 | 0.003575 | 598.63756 | 38.62212 | 0.576491 |
| 32 | 342.74444 | 0.003547 | 74.15071 | 38.8267 | 0.558924 |
| 34 | 1.747.428 | 0.003651 | 389.13522 | 37.52605 | 0.526933 |
| 36 | 5.280.47691 | 0.003727 | 1.200.44234 | 36.55648 | 0.49855 |
| 47 | 712.23964 | 0.004101 | 178.15474 | 32.03806 | 0.386359 |
| 50 | 95.26696 | 0.003098 | 17.99941 | 41.91809 | 0.364538 |
| 56 | 1.092.68136 | 0.004453 | 296.77759 | 28.40682 | 0.328157 |
| 62 | 840.35969 | 0.005024 | 257.49952 | 24.44474 | 0.299124 |
| 66 | 99.45693 | 0.005923 | 35.92909 | 20.28709 | 0.282866 |
| 67 | 646.06498 | 0.00544 | 214.3531 | 21.9627 | 0.279126 |
| 69 | 281.14625 | 0.005339 | 91.54925 | 22.11578 | 0.271996 |

Table S2
Comparison of kinetic studies

| Catalyst | Pseudo-first-order | | | | Pseudo-second-order | | |
|---|---|---|---|---|---|---|---|
| | $q_{e,exp.}$ (mg g$^{-1}$) | $K_1$ (min$^{-1}$) | $q_e$ (mg g$^{-1}$) | $R^2$ | $K_2$ (min$^{-1}$) | $q_e$ (mg g$^{-1}$) | $R^2$ |
| Acid Violet 49 | 0.00362 | 0.044 | 1.436 | 0.9619 | 0.010 | 5.64 | 0.3733 |
| Acid Blue 45 | 0.0638 | 0.040 | 1.288 | 0.9786 | $4.94 \times 10^{-4}$ | 109.8 | 0.2818 |

Table S3
Characteristics of Acid Violet 49 and Acid Blue 45

| Sr. no. | Pollutant | Other name | Structure | Molecular formula | $\lambda_{max}$ | C.I. |
|---|---|---|---|---|---|---|
| 1 | Acid Violet 49 | Acid Violet 6B |  | $C_{39}H_{40}N_3NaO_6S_2$ | 550 nm | 42640 |
| 2 | Acid Blue 45 | Acid Blue 2B |  | $C_{14}H_8N_2Na_2O_{10}S_2$ | 590 nm | 63010 |